

# Tell-Tale Watermarks for Explanatory Reasoning in Synthetic Media Forensics

Ching-Chun Chang and Isao Echizen

**Abstract**—The rise of synthetic media has blurred the boundary between reality and fabrication under the evolving power of artificial intelligence, fueling an infodemic that erodes public trust in cyberspace. For digital imagery, a multitude of editing applications further complicates the forensic analysis, including semantic edits that alter content, photometric adjustments that recalibrate colour characteristics, and geometric projections that reshape viewpoints. Collectively, these transformations manipulate and control perceptual interpretation of digital imagery. This susceptibility calls for forensic enquiry into reconstructing the chain of events, thereby revealing deeper evidential insight into the presence or absence of criminal intent. This study seeks to address an inverse problem of tracing the underlying generation chain that gives rise to the observed synthetic media. A tell-tale watermarking system is developed for explanatory reasoning over the nature and extent of transformations across the lifecycle of synthetic media. Tell-tale watermarks are tailored to different classes of transformations, responding in a manner that is neither strictly robust nor fragile but instead interpretable. These watermarks function as reference clues that evolve under the same transformation dynamics as the carrier media, leaving interpretable traces when subjected to transformations. Explanatory reasoning is then performed to infer the most plausible account across the combinatorial parameter space of composite transformations. Experimental evaluations demonstrate the validity of tell-tale watermarking with respect to fidelity, synchronicity and traceability.

## I. INTRODUCTION

**S**YNTHETIC media has come to blur the boundary between real and fabricated information, under the ever-evolving power of artificial intelligence (AI) [1]–[6]. When falling into the wrong hands, these technologies are capable of creating persuasive visual, auditory and linguistic content that deceives human sensory perception and even manipulates collective memory [7]–[14]. Over time, the very foundation of public trust in digital media erodes under the deluge of misinformation that sweeps through cyberspace, culminating in an infodemic [15]–[18].

In response, synthetic media forensics has emerged as a branch of science dedicated to the analysis of media authenticity, often in connection with cybercrimes [19]–[22]. Forensic paradigms can be broadly classified as either reactive, addressing problems after they arise, or proactive, anticipating and preventing them. Reactive forensics often relies on perceptual artefacts or statistical anomalies to identify synthetic media [23]–[28]. However, its reliability is undermined by the challenge of keeping pace with the growing sophistication of

forges [29]–[37]. In contrast, proactive forensics takes prior precautions to protect media at the time of creation [38]. It is typically associated with digital watermarking, the practice of imperceptibly embedding information into carrier media to serve a range of forensic purposes. The design philosophies underlying digital watermarking are shaped by the application context, which determines the expected response of watermarks to attacks on their carriers [39]–[44]. At one extreme, robust watermarks are designed to remain resilient against noise and distortion during transmission and dissemination, serving the purpose of source verification [45]–[52]. At the other extreme, fragile watermarks are engineered to disappear or be destroyed under modifications, serving the purpose of tamper detection [53]–[59].

Beyond basic forensic aims, a deeper quest lies in tracing the generation chain of synthetic media, uncovering the causal link between observable evidence and the latent sequence of operations from which it arose. In the case of visual media, the generation chain may encompass a wide spectrum of transformations, including semantic edits that alter objects within digital imagery, photometric adjustments that recalibrate colour characteristics, and geometric projections that reshape viewpoints. Such content synthesis and image enhancement processes can collectively control the perceptual interpretation of images. Establishing traceability allows forensic investigation to uncover deeper evidential insight into the presence or absence of criminal intent [60]–[65].

This task is inherently an inverse problem, where consequences are observable but causes are to be inferred. In classical logic, deduction infers the consequence from a known rule and an observed cause, whereas induction infers the rule from observed causes and their corresponding consequences. In contrast, the reasoning applied in this context is abduction, which infers the most plausible cause from an observed consequence along with a known rule [66]. It is a form of explanatory reasoning, also referred to as inference to the best explanation [67]. This concept is eloquently captured in Sir Arthur Conan Doyle’s *A Study in Scarlet*, voiced through Sherlock Holmes:

*Most people, if you describe a train of events to them, will tell you what the result would be. They can put those events together in their minds, and argue from them that something will come to pass. There are few people, however, who, if you told them a result, would be able to evolve from their own inner consciousness what the steps were which led up to that result. This power is what I mean when I talk of reasoning backwards, or analytically.*

C.-C. Chang and I. Echizen are with the Information and Society Research Division, National Institute of Informatics, Tokyo, Japan.

Correspondence: C.-C. Chang (email: ccchang@nii.ac.jp)

In this study, we develop tell-tale watermarks for explanatory reasoning over the generation chain of synthetic images, encompassing semantic, photometric and geometric transformations. Distinct from robust and fragile watermarks, tell-tale watermarks are designed to respond in a manner that is neither strictly robust nor fragile, but instead interpretable [68]. Transformations applied to the carrier media leave interpretable traces within the watermarks, which can subsequently be used to infer the nature and the extent of the transformations. We design tell-tale watermarks tailored to different classes of transformations and construct neural networks for encoding and decoding them into and from the carrier media. Explanatory reasoning is performed via combinatorial optimisation over the parameter space, yielding the most plausible hypothesis that explains the traces in the tell-tale watermarks. The validity of the proposed tell-tale watermarking system is verified through experimental evaluations with respect to fidelity, synchronicity and traceability.

The remainder of this paper is organised as follows. Section II formalises the problem and scope of this study. Section III presents the methodology of tell-tale watermarking and explanatory reasoning. Section IV provides the implementation details and evaluates the system performance in terms of fidelity, synchronicity and traceability. Section V concludes the paper and outlines potential directions for future research.

## II. PRELIMINARIES

The inverse problem of inferring parameterised transformation sequences from observed synthetic media is formalised with a note on intractability, followed by the scope of semantic, photometric and geometric transformations considered in this study.

### A. Problem Formulation

Let  $\mathcal{X}$  denote the space of digital images. We consider a set of parameterised transformation functions defined as

$$\mathcal{F} = \{f_{\vartheta_i} : \mathcal{X} \rightarrow \mathcal{X} \mid \vartheta_i \in \Theta_i\}, \quad (1)$$

where each function  $f_{\vartheta_i}$  represents a distinct type of image transformation and its effect is governed by a parameter  $\vartheta_i$  drawn from a specific parameter space  $\Theta_i$ . In practice, real-world manipulations seldom result from a single isolated transformation; rather, they often arise through the composite layering of multiple transformations, which collectively induce complex and diverse effects on digital images. To model such compositions, we define  $\mathcal{F}^*$  as the set of all finite ordered sequences of zero or more transformations from  $\mathcal{F}$  (the free monoid over  $\mathcal{F}$ ), given by

$$\mathcal{F}^* = \bigcup_{n \geq 0} \mathcal{F}^n, \quad (2)$$

where  $\mathcal{F}^n$  denotes the set of all sequences of  $n$  transformations drawn from  $\mathcal{F}$  (with repetition allowed) and  $\mathcal{F}^0$  contains the identity transformation which leaves images unchanged. Each sequence  $\mathbf{f} = (f_1, \dots, f_n) \in \mathcal{F}^*$  represents a composition of  $n$  transformations such that

$$\mathbf{f}(\mathbf{x}) = f_n \circ \dots \circ f_1(\mathbf{x}). \quad (3)$$

Note that the transformations are not necessarily commutative, meaning the order in which they are applied matters and changes the final outcome. Our objective is to reason inversely: given an observed image  $\tilde{\mathbf{x}}$ , we aim to infer a plausible sequence of parameterised transformations that may have been applied to an original image  $\mathbf{x} \in \mathcal{X}$ . Formally, we seek a hypothetical composite transformation  $\hat{\mathbf{f}} \in \mathcal{F}^*$  that best explains the given observation  $\tilde{\mathbf{x}}$ , by solving the following inverse problem

$$\hat{\mathbf{f}} = \arg \min_{\mathbf{f} \in \mathcal{F}^*} \mathcal{L}(\mathbf{f}(\mathbf{x}), \tilde{\mathbf{x}}), \quad (4)$$

where  $\mathcal{L}$  denotes a loss function evaluating how well the hypothesised reconstruction approximates the observation. However, the inverse problem defined above is generally ill-posed due to the unavailability of the original source  $\mathbf{x}$ . This renders the optimisation problem intractable in its current form, as the loss cannot be evaluated without access to the source. To address this limitation, we develop tell-tale watermarks, serving as reference clues that evolve under the same transformation dynamics as the original source. The inverse problem can thus be reformulated as

$$\hat{\mathbf{f}} = \arg \min_{\mathbf{f} \in \mathcal{F}^*} \mathcal{L}(\mathbf{f}(\mathbf{w}), \tilde{\mathbf{w}} + \epsilon), \quad (5)$$

where  $\tilde{\mathbf{w}}$  denotes the ideally transformed reference watermarks under the same parameterised transformations applied to the source, and  $\epsilon$  accounts for discrepancies arising from imperfect extraction or from incomplete synchronisation with the transformation dynamics. This mirroring behaviour enables explanatory reasoning in the absence of the original source.

### B. Transformations

Digital images, originating either from camera sensors or generative models, are often subjected to a range of transformations as they propagate through cyberspace. Such transformations can be applied manually by humans or autonomously by modern AI agents. Given high-level language instructions, an agent can select and execute transformations via in-built tools or generated codes. The scope of this study focuses on three broad classes of image editing: semantic, photometric, and geometric transformations.

*Semantic Transformations:* Semantic transformations synthesise content in the designated regions of an image. In this study, we consider semantic editing in the form of inpainting with generative models. Conditioned on a mask and a text prompt, the designated regions are filled with synthetic content.

*Photometric Transformations:* Photometric transformations adjust how content is perceived in terms of colour characteristics. They are commonly used for image enhancement, recalibrating colour balances to improve visual interpretation for particular applications. In this study, we consider adjustments of typical components, including brightness, contrast, hue and saturation.

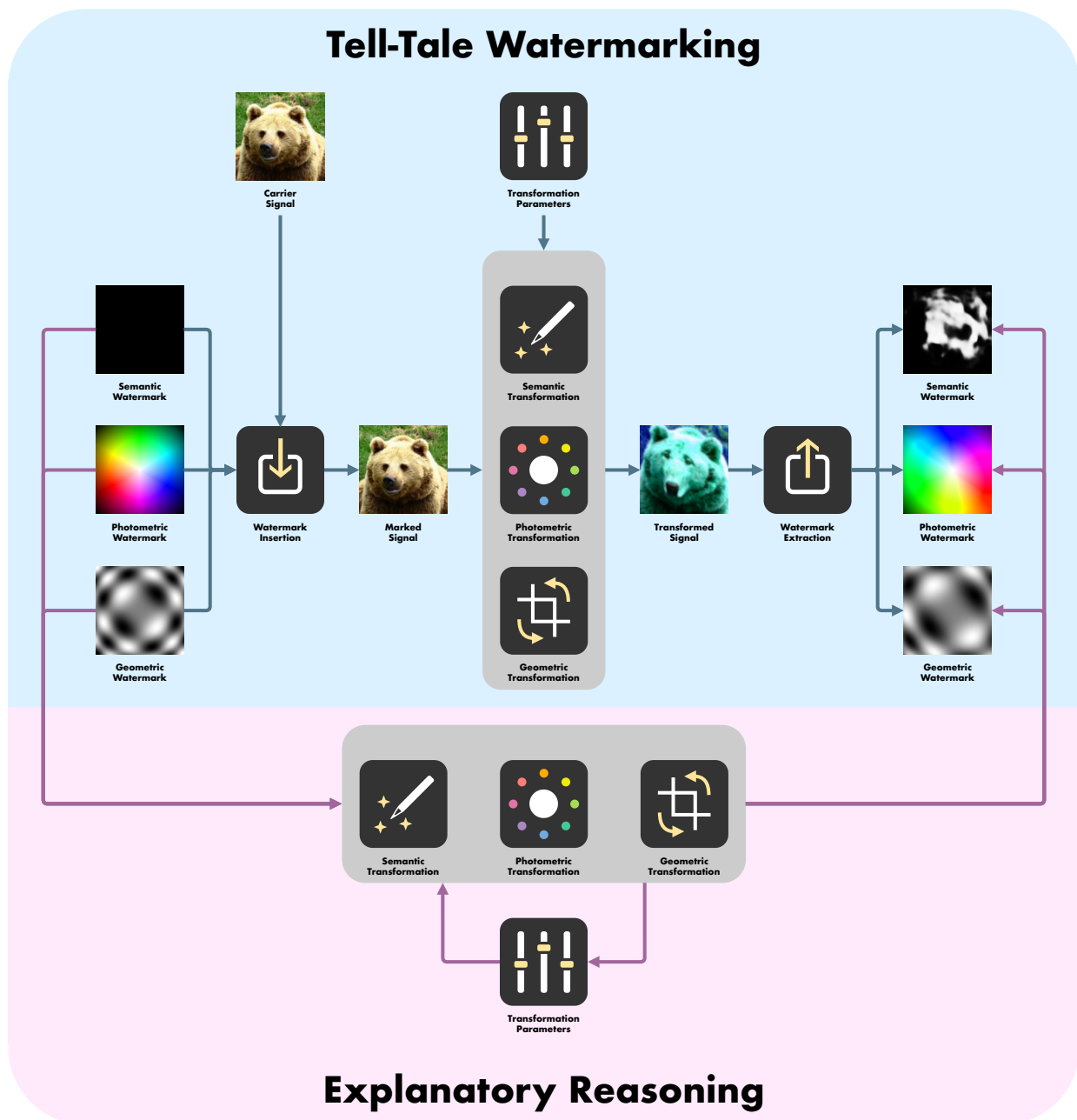


Fig. 1. Overview of tell-tale watermarking and explanatory reasoning in response to semantic, photometric and geometric transformations.

*Geometric Transformations:* Geometric transformations change how content is perceived in terms of the viewpoint. They reshape the spatial arrangement of pixels, aligning images to a desired projection surface or shape. In this study, we consider classic transformations from the affine family, including rotation, translation, scaling and shearing.

### III. METHODOLOGY

The methodology of our study is organised as follows. Watermark creation establishes tell-tale patterns whose responses to transformations are interpretable and measurable. Watermark insertion and extraction are performed by a pair of encoder and decoder, jointly optimised under simulated transformations, to embed watermarks with minimal perceptual

distortion of the carrier signal and maximal synchronicity with the applied transformations. Explanatory reasoning interprets the extracted watermarks, inferring the parameters of the applied transformations. An overview of the proposed method is outlined in Figure 1.

#### A. Watermark Creation

The creation of tell-tale watermarks requires tailored reference patterns whose responses to transformations are interpretable and measurable. Their designs varies by transformation type: semantic watermarks as a blank canvas sensitive to content edits, photometric watermarks as a colour wheel reflecting colour adjustments, and geometric watermarks as wave

---

**Algorithm 1** Watermark Creation
 

---

▷ *initialisation (polar coordinates)*

**for** each  $(x, y)$  **do**  
 $\bar{x} \leftarrow 2x/\text{width} - 1$   
 $\bar{y} \leftarrow 2y/\text{height} - 1$   
 $\varrho(x, y) \leftarrow \sqrt{\bar{x}^2 + \bar{y}^2}$   
 $\varphi(x, y) \leftarrow \text{atan2}(\bar{y}, \bar{x})$   
**end for**

▷ *semantic watermark (blank canvas)*

**for** each  $(x, y)$  **do**  
 $\mathbf{w}_{\text{sem}}(x, y) \leftarrow 0$   
**end for**

▷ *photometric watermark (colour wheel)*

**for** each  $(x, y)$  **do**  
 $h \leftarrow ((\varphi(x, y) + \Delta\varphi)/2\pi) \bmod 1$   
 $l \leftarrow 1 - \varrho(x, y)/\sqrt{2}$   
 $s \leftarrow 1$   
 $\mathbf{w}_{\text{pho}}(x, y) = (r, g, b) \leftarrow (h, l, s)$   
**end for**

▷ *geometric watermark (wave interference)*

**for** each  $(x, y)$  **do**  
 $\xi(x, y) \leftarrow \xi_{\min} + (\xi_{\max} - \xi_{\min}) \cdot \varrho(x, y)/\sqrt{2}$   
 $\omega(x, y) \leftarrow 2\pi \cdot \xi(x, y)$   
 $\Psi(x, y) \leftarrow \sin(\omega(x, y) \cdot x) \cdot \sin(\omega(x, y) \cdot y)$   
 $\mathbf{w}_{\text{geo}}(x, y) \leftarrow (1 + \Psi(x, y))/2$   
**end for**

---

interference pattern exposing affine distortions, as formulated in Algorithm 1.

*Semantic Watermark:* A semantic watermark is constructed as a blank canvas. Its simplicity allows any non-trivial semantic alteration to leave a discernible trace upon it. Let height and width denote the dimensions of the watermark and  $(x, y)$  denote pixel coordinates, where  $x \in \{1, \dots, \text{height}\}$  and  $y \in \{1, \dots, \text{width}\}$ . The semantic watermark is specified by

$$\mathbf{w}_{\text{sem}}(x, y) = 0 \quad \forall (x, y). \quad (6)$$

*Photometric Watermark:* A photometric watermark is constructed as a colour wheel whose behaviour under photometric transformations (brightness, contrast, saturation, hue) is predictable and easy to measure. In particular, it is designed as a circular spectrum in HLS colour space such that hue varies azimuthally with the angle around the centre, lightness decays radially with distance from the centre, and saturation remains spatially constant. Let  $(\bar{x}, \bar{y})$  denote the normalised pixel coordinates, centred at  $(0, 0)$  and ranging within  $[-1, 1]$ , defined by

$$\bar{x} = \frac{2x}{\text{width}} - 1, \quad \bar{y} = \frac{2y}{\text{height}} - 1. \quad (7)$$

The corresponding polar coordinates are derived as

$$\varrho(x, y) = \sqrt{\bar{x}^2 + \bar{y}^2}, \quad \varphi(x, y) = \text{atan2}(\bar{y}, \bar{x}). \quad (8)$$

where  $\varrho$  measures the distance from the centre and  $\varphi$  measures the angle around the centre. The hue channel is defined as

$$h(x, y) = \left( \frac{\varphi(x, y) + \Delta\varphi}{2\pi} \right) \bmod 1, \quad (9)$$

where  $\Delta\varphi \in \mathbb{R}$  is a user-defined angular shift specifying the default hue rotation. The division by  $2\pi$  converts an angle measured in radians into a fraction of a full cycle, whereas the modulo operation restricts the hue value to the interval  $[0, 1]$ . The lightness channel is defined as

$$l(x, y) = 1 - \frac{\varrho(x, y)}{\sqrt{2}}. \quad (10)$$

The division by  $\sqrt{2}$  scales  $\varrho$  from  $[0, \sqrt{2}]$  to  $[0, 1]$ , so that the centre ( $\varrho = 0$ ) attains maximum brightness ( $l = 1$ ) and the corners ( $\varrho = \sqrt{2}$ ) approach minimum brightness ( $l = 0$ ). The saturation channel is set as a constant value  $s(\bar{x}, \bar{y}) = 1$ . Finally, the photometric watermark is obtained by combining the hue, lightness and saturation channels and converting them to RGB colour space

$$\mathbf{w}_{\text{pho}}(x, y) = (r, g, b) \leftarrow (h, l, s). \quad (11)$$

*Geometric Watermark:* A geometric watermark is constructed as a wave interference pattern whose behaviour under geometric transformations (rotation, translation, scaling, shear) is regular and quantifiable. In particular, it is formed by the interference of two sinusoidal waves along the horizontal and vertical axes, with oscillatory frequency increasing radially from the centre. Let  $\varrho(x, y)$  denote the radial distance from the centre, obtained by converting the normalised coordinates into polar form. The spatial frequency is specified as

$$\xi(x, y) = \xi_{\min} + (\xi_{\max} - \xi_{\min}) \cdot \frac{\varrho(x, y)}{\sqrt{2}}, \quad (12)$$

where  $\xi_{\min}$  and  $\xi_{\max}$  are user-defined minimum and maximum frequencies, respectively. The division by  $\sqrt{2}$  scales  $\varrho$  from  $[0, \sqrt{2}]$  to  $[0, 1]$ , thereby assigning the minimum frequency to the centre ( $\varrho = 0$ ) and the maximum frequency to the corners ( $\varrho = \sqrt{2}$ ). The angular frequency is derived by multiplying the spatial frequency with a full cycle ( $2\pi$  radians)

$$\omega(x, y) = 2\pi\xi(x, y) \quad (13)$$

The wave interference pattern is then generated by the product of two orthogonal sinusoidal gratings

$$\Psi(x, y) = \sin(\omega(x, y)x) \cdot \sin(\omega(x, y)y). \quad (14)$$

Finally, the geometric watermark is obtained by normalising the wave interference pattern from  $[-1, 1]$  to  $[0, 1]$

$$\mathbf{w}_{\text{geo}}(x, y) = \frac{1 + \Psi(x, y)}{2}. \quad (15)$$

---

**Algorithm 2** Watermark Insertion & Extraction
 

---

▷ *Initialisation (learning & inference)*  
 (learning) for each  $\mathbf{x} \in \mathcal{X}_{\text{learn}}$  do the following  
 (inference) for each  $\mathbf{x} \in \mathcal{X}_{\text{infer}}$  do the following

▷ *watermark insertion (learning & inference)*  
 $\mathbf{x}_w \leftarrow \mathcal{E}(\mathbf{x}, \mathbf{w})$   
 where  $\mathbf{w} = [\mathbf{w}_{\text{sem}}, \mathbf{w}_{\text{pho}}, \mathbf{w}_{\text{geo}}]$

▷ *random transformations (learning & inference)*  
 sample  $(\mathbf{f}_{\text{sem}}, \mathbf{f}_{\text{pho}}, \mathbf{f}_{\text{geo}})$  randomly  
 (with random selection, intra-class ordering and parameters)  
 $\tilde{\mathbf{x}}_w \leftarrow \mathbf{f}_{\text{geo}}(\mathbf{f}_{\text{pho}}(\mathbf{f}_{\text{sem}}(\mathbf{x}_w)))$   
 (learning)  $\mathbf{f}_{\text{sem}}(\mathbf{x}_w) = (1 - \mathbf{m}) \cdot \mathbf{x}_w + \mathbf{m} \cdot \tilde{\mathbf{x}}_{\text{gen}}$   
 (inference)  $\mathbf{f}_{\text{sem}}(\mathbf{x}_w) = (1 - \mathbf{m}) \cdot \mathbf{x}_w + \mathbf{m} \cdot \mathbf{x}_{\text{gen}}$

▷ *watermark extraction (learning & inference)*  
 $\hat{\mathbf{w}} \leftarrow \mathcal{D}(\tilde{\mathbf{x}}_w)$   
 where  $\hat{\mathbf{w}} = [\hat{\mathbf{w}}_{\text{sem}}, \hat{\mathbf{w}}_{\text{pho}}, \hat{\mathbf{w}}_{\text{geo}}]$

▷ *ground-truth watermarks (learning)*  
 $\tilde{\mathbf{w}}_{\text{sem}} \leftarrow \mathbf{f}_{\text{geo}}(\mathbf{f}_{\text{sem}}(\mathbf{w}_{\text{sem}})) = \mathbf{f}_{\text{geo}}(\mathbf{m})$   
 $\tilde{\mathbf{w}}_{\text{pho}} \leftarrow \mathbf{f}_{\text{geo}}(\mathbf{f}_{\text{pho}}(\mathbf{w}_{\text{pho}}))$   
 $\tilde{\mathbf{w}}_{\text{geo}} \leftarrow \mathbf{f}_{\text{geo}}(\mathbf{w}_{\text{geo}})$   
 $\tilde{\mathbf{w}} \leftarrow [\tilde{\mathbf{w}}_{\text{sem}}, \tilde{\mathbf{w}}_{\text{pho}}, \tilde{\mathbf{w}}_{\text{geo}}]$

▷ *loss functions (learning)*  
 $\mathcal{L}_{\mathcal{E}}(\mathbf{x}_w, \mathbf{x}) \leftarrow \|\mathbf{x}_w - \mathbf{x}\|_1 + \|\mathbf{x}_w - \mathbf{x}\|_{\infty}$   
 $\mathcal{L}_{\mathcal{D}}(\hat{\mathbf{w}}, \tilde{\mathbf{w}}) \leftarrow \sum_{\text{xform}} \|\hat{\mathbf{w}}_{\text{xform}} - \tilde{\mathbf{w}}_{\text{xform}}\|_1$   
 where  $\text{xform} \in \{\text{sem}, \text{pho}, \text{geo}\}$   
 $\mathcal{L} \leftarrow \mathcal{L}_{\mathcal{E}} + \mathcal{L}_{\mathcal{D}}$

▷ *joint optimisation (learning)*  
 update  $\mathcal{E}$  via backpropagation of gradient  $\nabla_{\mathcal{E}} \mathcal{L}$   
 update  $\mathcal{D}$  via backpropagation of gradient  $\nabla_{\mathcal{D}} \mathcal{L}$

---

### B. Watermark Insertion & Extraction

Watermark insertion and extraction are performed by two respective neural networks trained jointly, with simulated transformations applied in between, as presented in Algorithm 2. Given a carrier image  $\mathbf{x}$  and a collection of tell-tale watermarks  $\mathbf{w} = (\mathbf{w}_{\text{sem}}, \mathbf{w}_{\text{pho}}, \mathbf{w}_{\text{geo}})$ , the encoder  $\mathcal{E}$  embeds  $\mathbf{w}$  into  $\mathbf{x}$ , producing a marked image

$$\mathbf{x}_w = \mathcal{E}(\mathbf{x}, \mathbf{w}). \quad (16)$$

A transformation sequence  $\mathbf{f} \in \mathcal{F}^*$  is then randomly instantiated and applied to the marked image, yielding a transformed image

$$\tilde{\mathbf{x}}_w = \mathbf{f}(\mathbf{x}_w). \quad (17)$$

We restrict attention to an ordered transformation chain that mirrors common practice in generative pipelines, defined as

$$\mathbf{f} = \mathbf{f}_{\text{geo}}(\mathbf{f}_{\text{pho}}(\mathbf{f}_{\text{sem}}(\mathbf{x}_w))), \quad (18)$$

where semantic editing  $\mathbf{f}_{\text{sem}}$  is performed first to modify content, photometric adjustment  $\mathbf{f}_{\text{pho}}$  follows to harmonise colour and suppress artefacts, and geometric projection  $\mathbf{f}_{\text{geo}}$

is performed last to control scale, orientation and viewpoint. This chain reduces the combinatorial complexity of parameter reasoning, albeit at the cost of generality. Nevertheless, full randomness is preserved within each class of transformations: brightness, contrast, hue and saturation are applied in random order for photometric transformations, while rotation, translation, scaling and shearing are likewise applied in random order for geometric transformations. For semantic editing, we formulate it as inpainting based on generative models tasked with filling the designated missing regions, conditioned on a mask  $\mathbf{m}$  and a text prompt. Direct semantic editing with generative models, however, is computationally intensive in the learning phase, as joint optimisation of encoder and decoder requires repeated iterations. To achieve efficiency, we replace it with a surrogate scheme that masks random regions and fills them with simulated alternatives, expressed as

$$\begin{aligned} \mathbf{f}_{\text{sem}}(\mathbf{x}_w \mid \mathbf{m}, \text{prompt}) &= (1 - \mathbf{m}) \cdot \mathbf{x}_w + \mathbf{m} \cdot \mathbf{x}_{\text{gen}}, \\ &\approx (1 - \mathbf{m}) \cdot \mathbf{x}_w + \mathbf{m} \cdot \tilde{\mathbf{x}}_{\text{gen}}, \end{aligned} \quad (19)$$

where  $\mathbf{x}_{\text{gen}}$  is generated content conditioned on a mask  $\mathbf{m}$  and a text prompt, and  $\tilde{\mathbf{x}}_{\text{gen}}$  denotes its simulated counterpart. In practice, we simulate the generated content by applying random photogeometric transformations to the image  $\mathbf{x}_w$ , such that the masked regions are filled with transformed variants of the image itself. From the transformed image  $\tilde{\mathbf{x}}_w$ , the decoder  $\mathcal{D}$  attempts to extract the watermark

$$\hat{\mathbf{w}} = \mathcal{D}(\tilde{\mathbf{x}}_w). \quad (20)$$

To preserve perceptual fidelity after watermark insertion, we define an encoding loss  $\mathcal{L}_{\mathcal{E}}(\mathbf{x}_w, \mathbf{x})$  that penalises deviations between the carrier image and its marked counterpart, given by

$$\mathcal{L}_{\mathcal{E}}(\mathbf{x}_w, \mathbf{x}) = \|\mathbf{x}_w - \mathbf{x}\|_1 + \|\mathbf{x}_w - \mathbf{x}\|_{\infty}. \quad (21)$$

where  $\ell_1$  norm captures global deviations and the  $\ell_{\infty}$  norm suppresses localised residual spikes. To support synchronicity with the applied transformations, we define a decoding loss that measures discrepancies between the extracted watermark and its ground truth counterpart, given by

$$\mathcal{L}_{\mathcal{D}}(\hat{\mathbf{w}}, \tilde{\mathbf{w}}) = \sum_{\text{xform}} \|\hat{\mathbf{w}}_{\text{xform}} - \tilde{\mathbf{w}}_{\text{xform}}\|_1, \quad (22)$$

where  $\text{xform} \in \{\text{sem}, \text{pho}, \text{geo}\}$  indicates the transformation types,  $\hat{\mathbf{w}}_{\text{xform}}$  is the extracted watermark and  $\tilde{\mathbf{w}}_{\text{xform}}$  denotes the target ground truth. We obtain the ground truth by transforming the reference watermarks with identical parameters to those applied to the carrier image, namely

$$\begin{aligned} \tilde{\mathbf{w}}_{\text{sem}} &= \mathbf{f}_{\text{geo}}(\mathbf{f}_{\text{sem}}(\mathbf{w}_{\text{sem}})), \\ \tilde{\mathbf{w}}_{\text{pho}} &= \mathbf{f}_{\text{geo}}(\mathbf{f}_{\text{pho}}(\mathbf{w}_{\text{pho}})), \\ \tilde{\mathbf{w}}_{\text{geo}} &= \mathbf{f}_{\text{geo}}(\mathbf{w}_{\text{geo}}). \end{aligned} \quad (23)$$

For the semantic transformation, the filled regions are flagged with 1s against the reference watermark initialised with 0s, and the resulting expression reduces to the editing mask

$$\begin{aligned} \mathbf{f}_{\text{sem}}(\mathbf{w}_{\text{sem}}) &= (1 - \mathbf{m}) \cdot \mathbf{w}_{\text{sem}} + \mathbf{m} \cdot \mathbf{1} \\ &= (1 - \mathbf{m}) \cdot \mathbf{0} + \mathbf{m} \cdot \mathbf{1} = \mathbf{m}. \end{aligned} \quad (24)$$

---

**Algorithm 3** Explanatory Reasoning
 

---

▷ *geometric reasoning*  
 $\mathbf{w}_{\text{geo}}$  and  $\hat{\mathbf{w}}_{\text{geo}}$  are given  
 $\vartheta_{\text{geo}} \leftarrow \text{default}$   
 $(\hat{\varpi}_{\text{geo}}, \hat{\vartheta}_{\text{geo}}) \leftarrow \text{none}; \text{iter} \leftarrow 0; L_{\min} \leftarrow \infty$   
**for** each  $\varpi_{\text{geo}} \in \text{Sym}(\{\text{ro, tr, sc, sh}\})$  **do**  
  **while**  $\text{iter} < \text{iter}_{\max}$  **do**  
     $\tilde{\mathbf{w}}_{\text{geo}} \leftarrow \mathbf{f}_{\text{geo}}(\mathbf{w}_{\text{geo}} \mid \varpi_{\text{geo}}, \vartheta_{\text{geo}})$   
     $\mathcal{L}_{\text{geo}} \leftarrow \|\tilde{\mathbf{w}}_{\text{geo}} - \hat{\mathbf{w}}_{\text{geo}}\|_1$   
    update  $(\varpi_{\text{geo}}, \vartheta_{\text{geo}})$  via backpropagation  
    **if**  $\mathcal{L}_{\text{geo}} < \mathcal{L}_{\min}$  **then**  
       $(\hat{\varpi}_{\text{geo}}, \hat{\vartheta}_{\text{geo}}) \leftarrow (\varpi_{\text{geo}}, \vartheta_{\text{geo}})$   
    **end if**  
     $\text{iter} \leftarrow \text{iter} + 1$   
  **end while**  
**end for**  
**return**  $(\hat{\varpi}_{\text{geo}}, \hat{\vartheta}_{\text{geo}})$

▷ *photometric reasoning*  
 $\mathbf{w}_{\text{pho}}$  and  $\hat{\mathbf{w}}_{\text{pho}}$  are given  
 $\vartheta_{\text{pho}} \leftarrow \text{default}$   
 $(\hat{\varpi}_{\text{pho}}, \hat{\vartheta}_{\text{pho}}) \leftarrow \text{none}; \text{iter} \leftarrow 0; L_{\min} \leftarrow \infty$   
**for** each  $\varpi_{\text{pho}} \in \text{Sym}(\{\text{b, c, h, s}\})$  **do**  
  **while**  $\text{iter} < \text{iter}_{\max}$  **do**  
     $\tilde{\mathbf{w}}_{\text{pho}} \leftarrow \mathbf{f}_{\text{geo}}(\mathbf{f}_{\text{pho}}(\mathbf{w}_{\text{geo}} \mid \varpi_{\text{pho}}, \vartheta_{\text{pho}}) \mid \hat{\varpi}_{\text{geo}}, \hat{\vartheta}_{\text{geo}})$   
     $\mathcal{L}_{\text{pho}} \leftarrow \|\tilde{\mathbf{w}}_{\text{pho}} - \hat{\mathbf{w}}_{\text{pho}}\|_1$   
    update  $(\varpi_{\text{pho}}, \vartheta_{\text{pho}})$  via backpropagation  
    **if**  $\mathcal{L}_{\text{pho}} < \mathcal{L}_{\min}$  **then**  
       $(\hat{\varpi}_{\text{pho}}, \hat{\vartheta}_{\text{pho}}) \leftarrow (\varpi_{\text{pho}}, \vartheta_{\text{pho}})$   
    **end if**  
     $\text{iter} \leftarrow \text{iter} + 1$   
  **end while**  
**end for**  
**return**  $(\hat{\varpi}_{\text{pho}}, \hat{\vartheta}_{\text{pho}})$

▷ *semantic reasoning*  
 $\mathbf{w}_{\text{sem}}$  and  $\hat{\mathbf{w}}_{\text{sem}}$  are given  
 $\hat{\vartheta}_{\text{sem}} \leftarrow \hat{\mathbf{w}}_{\text{sem}}$   
**return**  $\hat{\vartheta}_{\text{sem}}$

---

The overall watermarking loss  $\mathcal{L}_{\mathcal{W}} = \mathcal{L}_{\mathcal{E}} + \mathcal{L}_{\mathcal{D}}$  is backpropagated to update both  $\mathcal{E}$  and  $\mathcal{D}$  jointly. This joint formulation encourages the inserted watermark to be minimally disruptive to the carrier image yet maximally reflective of the applied transformations.

### C. Explanatory Reasoning

Explanatory reasoning concerns the estimation of transformation parameters based on the tell-tale traces left within the extracted watermarks. The procedures and objectives vary by transformation type: geometric reasoning determines affine distortions, photometric reasoning infers colour adjustments, and semantic reasoning identifies edited regions, as detailed in Algorithm 3.

*Geometric Reasoning:* Geometric reasoning aims to determine the ordering and parameters such that the composite geometric transformation  $\mathbf{f}_{\text{geo}}$  maps the reference watermark  $\mathbf{w}_{\text{geo}}$  as closely as possible to the extracted watermark  $\hat{\mathbf{w}}_{\text{geo}}$ . Let the hypothesised transformed watermark be denoted by

$$\tilde{\mathbf{w}}_{\text{geo}} = \mathbf{f}_{\text{geo}}(\mathbf{w}_{\text{geo}} \mid \varpi_{\text{geo}}, \vartheta_{\text{geo}}) \quad (25)$$

where  $\varpi_{\text{geo}}$  specifies the permutation ordering of rotation, translation, scaling and shearing, and  $\vartheta_{\text{geo}}$  contains their respective parameters, defined as

$$\begin{aligned} \varpi_{\text{geo}} &\in \text{Sym}(\{\text{ro, tr, sc, sh}\}), \\ \vartheta_{\text{geo}} &= [\vartheta_{\text{ro}}, \vartheta_{\text{tr}}^x, \vartheta_{\text{tr}}^y, \vartheta_{\text{sc}}, \vartheta_{\text{sh}}^x, \vartheta_{\text{sh}}^y]. \end{aligned} \quad (26)$$

The rotation parameter  $\vartheta_{\text{ro}}$  is the clockwise angle (in radians), the translation parameters  $\vartheta_{\text{tr}}^x$  and  $\vartheta_{\text{tr}}^y$  are horizontal and vertical fractions of the width and height, the scaling parameter  $\vartheta_{\text{sc}}$  is the scale factor, and the shearing parameters  $\vartheta_{\text{sh}}^x$  and  $\vartheta_{\text{sh}}^y$  are clockwise angles with respect to the horizontal and vertical axes (in radians). The reasoning task is therefore to jointly resolve both the ordering and the magnitudes of the underlying geometric distortions, expressed as a nested optimisation

$$\hat{\varpi}_{\text{geo}}, \hat{\vartheta}_{\text{geo}} = \arg \min_{\varpi_{\text{geo}}} \min_{\vartheta_{\text{geo}}} \|\tilde{\mathbf{w}}_{\text{geo}} - \hat{\mathbf{w}}_{\text{geo}}\|_1. \quad (27)$$

Geometric transformations can be viewed as projections between coordinate spaces. A sampling grid is constructed to map each output pixel to its source location, from which pixel values are sampled through interpolation. Specifically, for each output pixel at  $(x, y)$ , its corresponding source coordinates  $(u, v)$  are computed by

$$\begin{bmatrix} u \\ v \\ 1 \end{bmatrix} = \mathbf{M} \begin{bmatrix} x \\ y \\ 1 \end{bmatrix}, \quad (28)$$

where the matrix  $\mathbf{M}$  is a recentred inverse affine matrix. The recentring process converts the standard inverse affine matrix  $\mathbf{M}_{\text{geo}}$  from the origin  $(0, 0)$  to the centre of the image, given by

$$\mathbf{M} = \begin{bmatrix} 1 & 0 & \text{centre}^x \\ 0 & 1 & \text{centre}^y \\ 0 & 0 & 1 \end{bmatrix} \mathbf{M}_{\text{geo}} \begin{bmatrix} 1 & 0 & -\text{centre}^x \\ 0 & 1 & -\text{centre}^y \\ 0 & 0 & 1 \end{bmatrix}, \quad (29)$$

where  $(\text{centre}^x, \text{centre}^y) = ((\text{width} - 1)/2, (\text{height} - 1)/2)$ . The standard inverse affine matrices for rotation, translation, scaling and shearing are defined respectively by

$$\begin{aligned} \mathbf{M}_{\text{ro}} &= \begin{bmatrix} \cos \vartheta_{\text{ro}} & -\sin \vartheta_{\text{ro}} & 0 \\ \sin \vartheta_{\text{ro}} & \cos \vartheta_{\text{ro}} & 0 \\ 0 & 0 & 1 \end{bmatrix}, \\ \mathbf{M}_{\text{tr}} &= \begin{bmatrix} 1 & 0 & -\vartheta_{\text{tr}}^x \text{width} \\ 0 & 1 & -\vartheta_{\text{tr}}^y \text{height} \\ 0 & 0 & 1 \end{bmatrix}, \\ \mathbf{M}_{\text{sc}} &= \begin{bmatrix} 1/\vartheta_{\text{sc}} & 0 & 0 \\ 0 & 1/\vartheta_{\text{sc}} & 0 \\ 0 & 0 & 1 \end{bmatrix}, \\ \mathbf{M}_{\text{sh}} &= \begin{bmatrix} 1 & \tan \vartheta_{\text{sh}}^x & 0 \\ \tan \vartheta_{\text{sh}}^y & 1 & 0 \\ 0 & 0 & 1 \end{bmatrix}. \end{aligned} \quad (30)$$

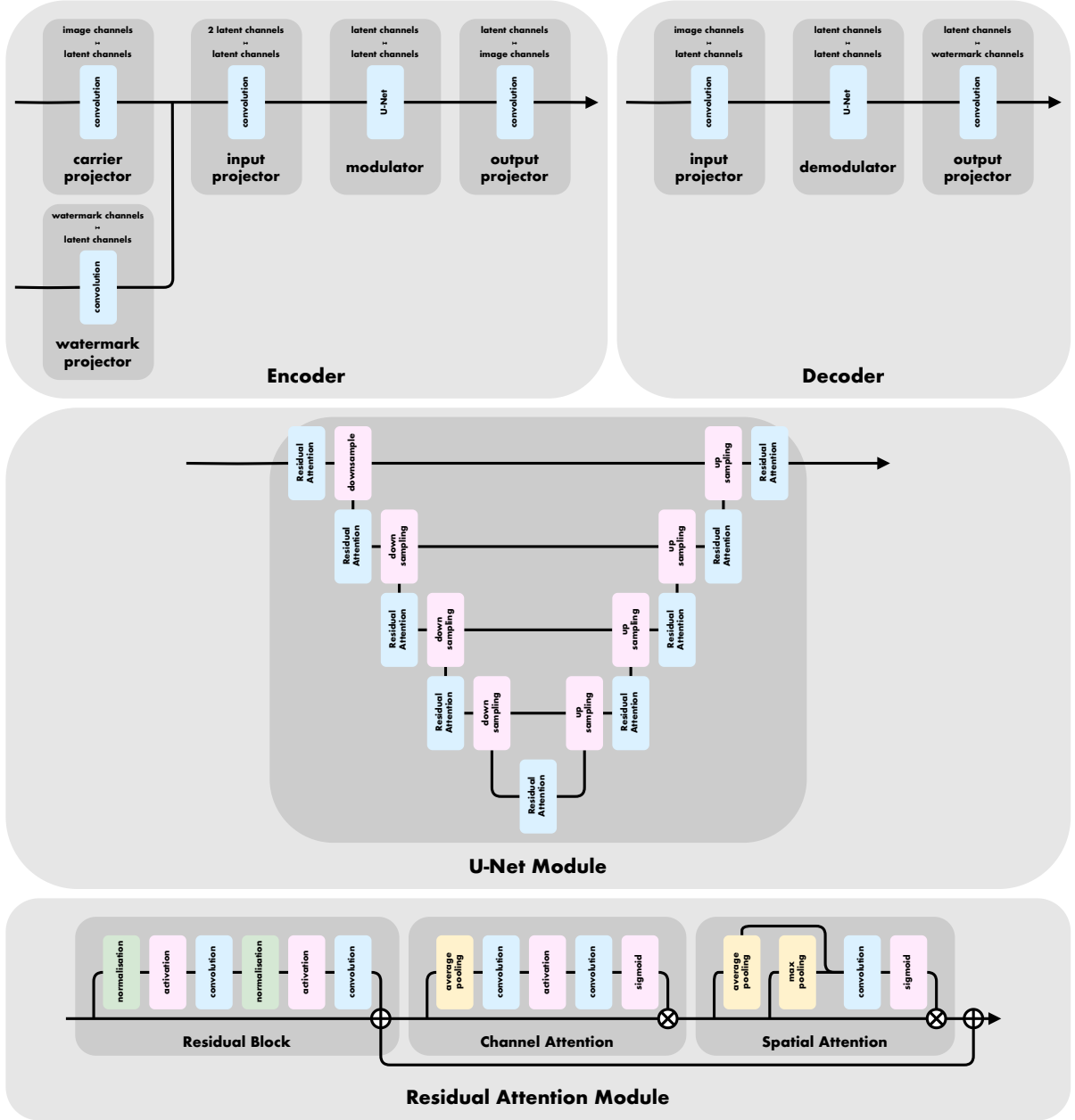


Fig. 2. Architecture of the encoder and decoder neural networks, with implementation details for the U-Net module and the residual attention module.

Since the coordinates  $(u, v)$  are not necessarily integer-valued, bilinear interpolation is applied and the transformed watermark is given by

$$\tilde{\mathbf{w}}_{\text{geo}}(x, y) = \sum_{\text{cor}} \beta_{\text{cor}} \cdot \mathbf{w}_{\text{geo}}(u_{\text{cor}}, v_{\text{cor}}), \quad (31)$$

where  $\text{cor} \in \{\text{nw}, \text{ne}, \text{sw}, \text{se}\}$  is the set of four corners (northwest, northeast, southwest and southeast),  $(u_{\text{cor}}, v_{\text{cor}})$  are integer-valued corner coordinates

$$\begin{aligned} (u_{\text{nw}}, v_{\text{nw}}) &= (\lfloor u \rfloor, \lfloor v \rfloor), \\ (u_{\text{ne}}, v_{\text{ne}}) &= (\lfloor u \rfloor + 1, \lfloor v \rfloor), \\ (u_{\text{sw}}, v_{\text{sw}}) &= (\lfloor u \rfloor, \lfloor v \rfloor + 1), \\ (u_{\text{se}}, v_{\text{se}}) &= (\lfloor u \rfloor + 1, \lfloor v \rfloor + 1), \end{aligned} \quad (32)$$

and  $\beta_{\text{cor}}$  are the corresponding bilinear interpolation weights

$$\begin{aligned} \beta_{\text{nw}} &= (u_{\text{se}} - u)(v_{\text{se}} - v), \\ \beta_{\text{ne}} &= (u - u_{\text{sw}})(v_{\text{sw}} - v), \\ \beta_{\text{sw}} &= (u_{\text{ne}} - u)(v - v_{\text{ne}}), \\ \beta_{\text{se}} &= (u - u_{\text{nw}})(v - v_{\text{nw}}). \end{aligned} \quad (33)$$

We set  $\tilde{\mathbf{w}}_{\text{geo}}(x, y)$  to zero if  $\mathbf{w}_{\text{geo}}(u_{\text{cor}}, v_{\text{cor}})$  does not exist due to out-of-bound coordinates.

*Photometric Reasoning:* Photometric reasoning seeks the ordering and parameters such that the composite photometric transformation  $\mathbf{f}_{\text{pho}}$ , when applied to the reference watermark  $\mathbf{w}_{\text{pho}}$  and subsequently calibrated by the composite geometric transformation  $\mathbf{f}_{\text{geo}}$  (with pre-estimated ordering  $\hat{\omega}_{\text{geo}}$  and parameters  $\hat{\theta}_{\text{geo}}$ ), produce a result that best aligns with the

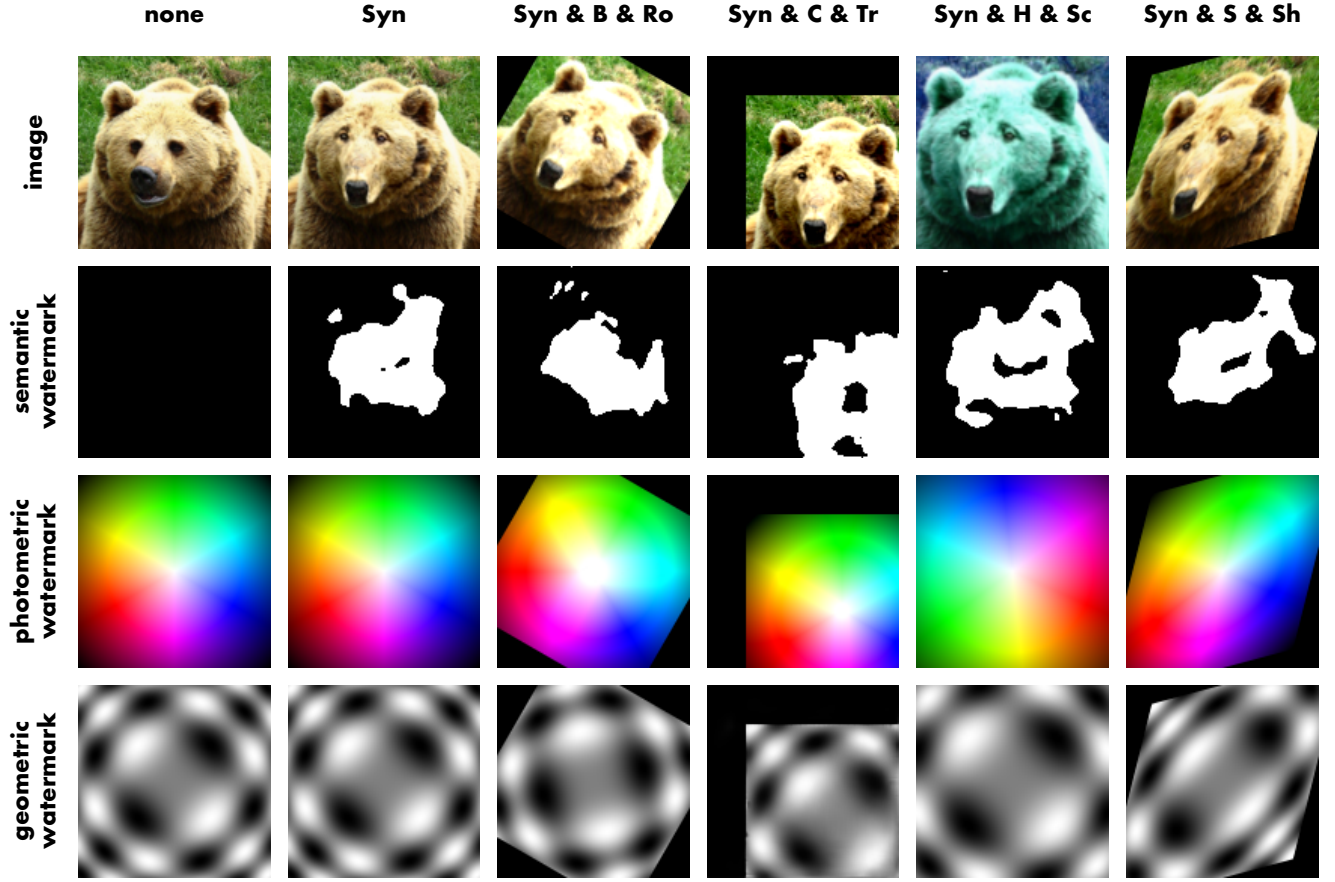


Fig. 3. Demonstration of tell-tale watermarks under different transformation chains.

extracted watermark  $\hat{\mathbf{w}}_{\text{pho}}$ . The hypothesised transformed watermark is expressed as

$$\tilde{\mathbf{w}}_{\text{pho}} = \mathbf{f}_{\text{geo}}(\mathbf{f}_{\text{pho}}(\mathbf{w}_{\text{pho}} | \varpi_{\text{pho}}, \vartheta_{\text{pho}}) | \hat{\omega}_{\text{geo}}, \hat{\vartheta}_{\text{geo}}), \quad (34)$$

where  $\varpi_{\text{pho}}$  represents the permutation ordering of brightness, contrast, hue and saturation adjustments, and  $\vartheta_{\text{pho}}$  comprises their respective parameters, defined as

$$\begin{aligned} \varpi_{\text{pho}} &\in \text{Sym}(\{b, c, h, s\}), \\ \vartheta_{\text{pho}} &= [\vartheta_b, \vartheta_c, \vartheta_h, \vartheta_s]. \end{aligned} \quad (35)$$

The reasoning task is thus to simultaneously infer the ordering and the magnitudes of the underlying photometric distortions, formulated as a nested optimisation

$$\hat{\varpi}_{\text{pho}}, \hat{\vartheta}_{\text{pho}} = \arg \min_{\varpi_{\text{pho}}} \min_{\vartheta_{\text{pho}}} \|\tilde{\mathbf{w}}_{\text{pho}} - \hat{\mathbf{w}}_{\text{pho}}\|_1. \quad (36)$$

The photometric transformations associated with brightness, contrast, hue and saturation are defined respectively as

$$\begin{aligned} f_{\vartheta_b}(\mathbf{w}_{\text{pho}}) &= \vartheta_b \mathbf{w}_{\text{pho}} + (1 - \vartheta_b) \mathbf{0}, \\ f_{\vartheta_c}(\mathbf{w}_{\text{pho}}) &= \vartheta_c \mathbf{w}_{\text{pho}} + (1 - \vartheta_c) \mu(\ell(\mathbf{w}_{\text{pho}})), \\ f_{\vartheta_h}(\mathbf{w}_{\text{pho}}) &= (\hat{r}, \hat{g}, \hat{b}) \leftarrow ((h + \vartheta_h) \bmod 1, s, v), \\ f_{\vartheta_s}(\mathbf{w}_{\text{pho}}) &= \vartheta_s \mathbf{w}_{\text{pho}} + (1 - \vartheta_s) \ell(\mathbf{w}_{\text{pho}}), \end{aligned} \quad (37)$$

where  $\mathbf{0}$  denotes the all-zero matrix,  $\mu$  denotes the mean operator,  $\ell$  denotes the luminance from grayscale conversion,

$(h, s, v)$  are the HSV components and  $(\hat{r}, \hat{g}, \hat{b})$  are the resulting RGB values. Specifically, brightness adjustment scales intensities relative to black, contrast adjustment varies intensities relative to their mean luminance, hue adjustment shifts the hue while keeping saturation and value fixed, and saturation adjustment interpolates between the colour image and its grayscale version.

*Semantic Reasoning:* Semantic reasoning aims to infer the spatial regions of content editing, taking the form of a matrix  $\vartheta_{\text{sem}}$ , in contrast to geometric and photometric transformations, which estimate finite-dimensional parameter vectors  $\vartheta_{\text{geo}}$  and  $\vartheta_{\text{pho}}$ . The edited regions are directly revealed by the extracted semantic watermark, without requiring additional computation; that is,  $\vartheta_{\text{sem}} = \tilde{\mathbf{w}}_{\text{sem}}$ . During the learning phase, the encoder and decoder are jointly trained to minimise the discrepancy between the extracted semantic watermark and the ground truth, expressed as  $\min \|\tilde{\mathbf{w}}_{\text{sem}} - \hat{\mathbf{w}}_{\text{sem}}\|_1$ , where the ground truth  $\tilde{\mathbf{w}}_{\text{sem}}$  corresponds to the editing mask after geometric transformation  $\mathbf{f}_{\text{geo}}(\mathbf{m})$ . Therefore, the extracted semantic watermark provides a direct indication of the regions subject to content editing.

#### IV. EVALUATION

The validity of tell-tale watermarking is evaluated through three aspects: watermark insertion assessed by fidelity, wa-

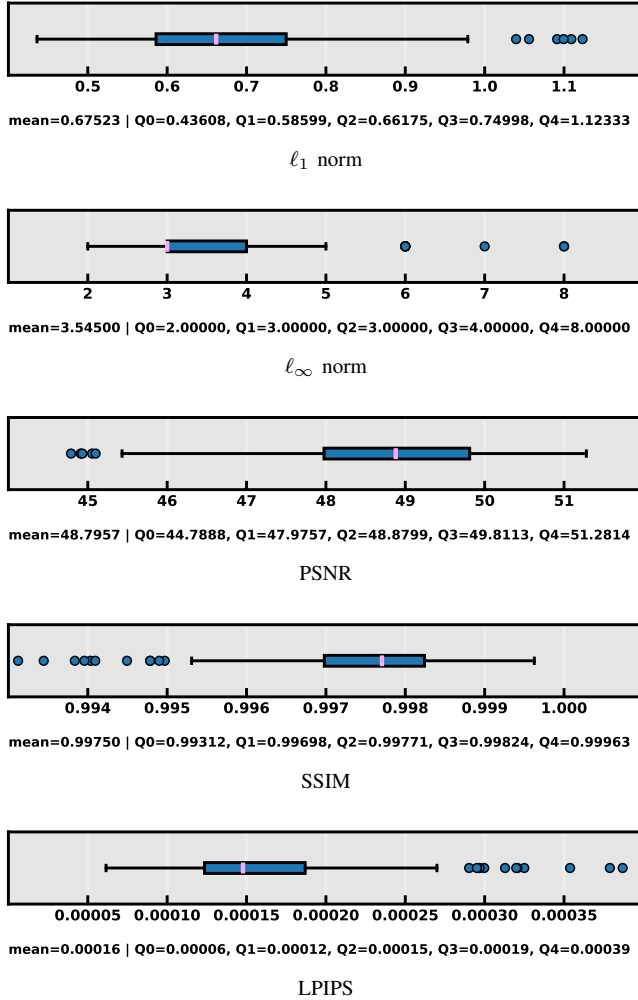


Fig. 4. Fidelity evaluation of watermark insertion based on distortion metrics between carrier and marked images.

termark extraction assessed by synchronicity, and explanatory reasoning assessed by traceability.

### A. Experimental Setup

Experiments are conducted on the COCO dataset (common objects in context) [69], partitioned for learning and inference, with all images resampled to a consistent resolution of  $128 \times 128$  pixels. The encoder and decoder are based on a U-Net architecture with residual and attention modules [70]–[72], where the number of base latent channels is configured as 32, as illustrated in Figure 2. Semantic editing is performed with a stable diffusion model prompted to synthesise realistic content in masked regions [73]. Photometric transformations are defined with brightness, contrast and saturation varied in  $[0.75, 1.25]$  (no adjustment at 1) and hue in  $[-0.35, 0.35]$  (no shift at 0). Geometric transformations include rotation in  $[-30^\circ, 30^\circ]$  (unchanged at  $0^\circ$ ), translation in  $[-0.2, 0.2]$  along both axes (unchanged at 0), scaling in  $[0.8, 1.2]$  (unchanged at 1) and shearing in  $[-15^\circ, 15^\circ]$  along both axes (unchanged at  $0^\circ$ ). Results in degrees are normalised to fractions of a full cycle. Explanatory reasoning of photometric and geometric parameters is performed with a maximum of 100 iterations,

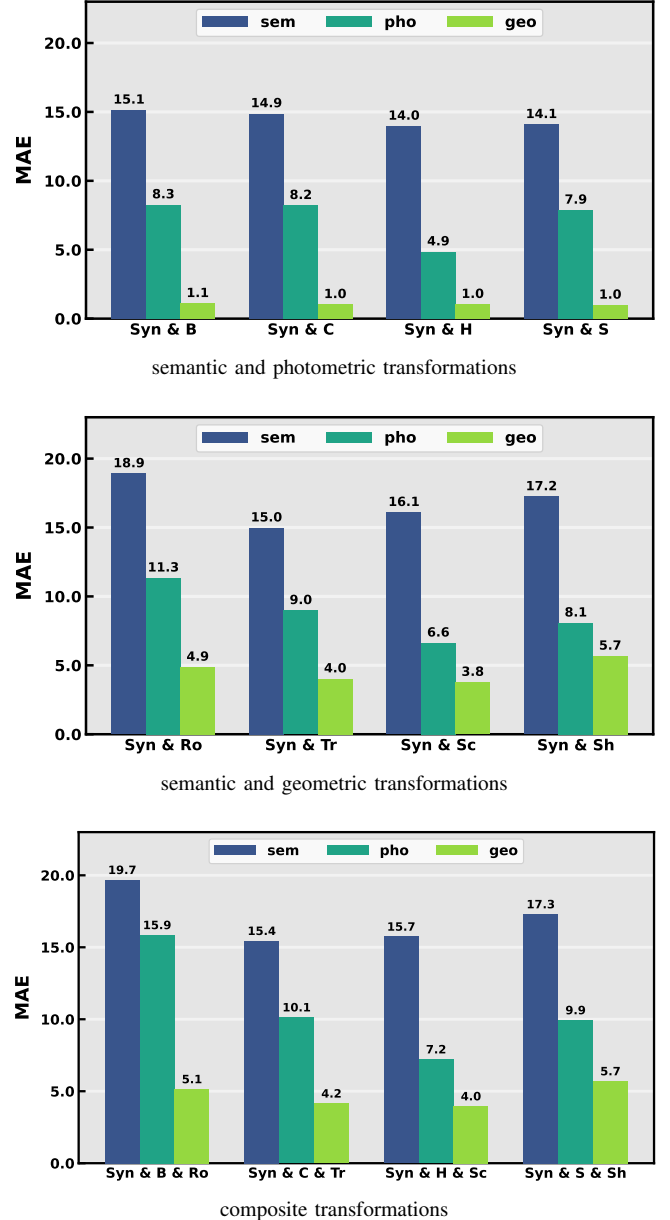


Fig. 5. Synchronicity evaluation of watermark extraction based on MAE between extracted and ground-truth watermarks.

using an update rate of 0.1. A visual demonstration of images and watermarks under composite transformations is shown in Figure 3.

### B. Fidelity

Fidelity measures perceptual similarity between carrier and marked images. We evaluate fidelity via the following quality metrics:  $l_1$  norm,  $l_\infty$  norm, peak signal-to-noise ratio (PSNR), structural similarity index measure (SSIM), and learnt perceptual image patch similarity (LPIPS), as shown in Figure 4. The  $l_1$  norm represents the average absolute pixel difference and the  $l_\infty$  norm captures the maximum absolute pixel deviation, where values close to zero signify negligible distortion. PSNR is defined via the ratio of the maximum possible pixel value to the noise, with satisfactory quality values typically between

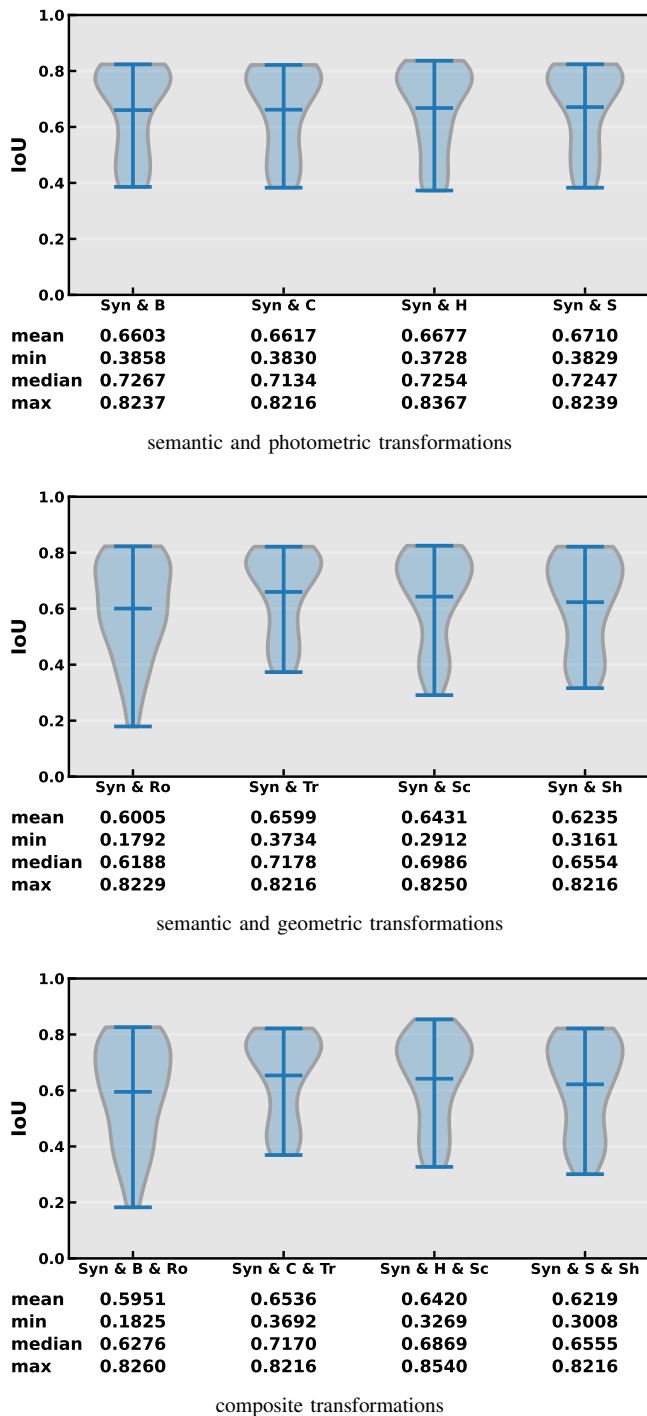


Fig. 6. Traceability evaluation of semantic reasoning based on IoU between estimated and true editing regions.

30 and 50 dB. SSIM compares structural similarity in terms of luminance, contrast and texture, with a score of one denoting identical images. LPIPS is a learning-based perceptual similarity measure for approximating human visual perception, with values close to zero regarded as nearly indistinguishable to human observers. The statistical results across these fidelity metrics demonstrate that watermark insertion introduces only negligible perceptual distortion to the carrier media.

### C. Synchronicity

Synchronicity characterises how closely the extracted watermarks follow the effects of transformations applied to the media, as reflected by their agreement with directly transformed ground-truth counterparts. We quantify synchronicity by the mean absolute error (MAE) between the extracted watermarks  $\hat{w}$  and their ground-truth counterparts  $\tilde{w}$ , as shown in Figure 5. For each marked image, we first apply a semantic transformation to synthesise content in a random region, followed by a photometric transformation for colour adjustment, a geometric transformation for perspective projection, or a composite transformation combining the two. Watermarks are then extracted from the transformed image and compared against their ground-truth counterparts, which are obtained by applying the same sequence of transformations directly to the initial reference watermarks. It is observed that composite transformations lead to greater degradation in synchronicity compared with applying a semantic transformation followed by either a photometric or a geometric transformation. The photometric watermark reflects changes in hue more faithfully than changes in brightness, contrast or saturation. The geometric watermark demonstrates relatively stable alignment with its ground-truth counterpart across rotation, translation, scaling and shearing. The geometric watermark achieves the highest synchronicity, followed by the photometric watermark and then the semantic watermark.

### D. Traceability

Traceability refers to the extent to which explanatory reasoning can correctly infer the parameters of transformations applied to the media from traces left within the extracted watermarks. A semantic transformation is first applied to synthesise content in a random region, followed by a photometric transformation, a geometric transformation, or a composite transformation combining the two. For semantic reasoning, we compare the extracted semantic watermark against the ground-truth mask through the intersection over union (IoU), as shown in Figure 6. The average IoU lies within the range of 0.6 to 0.7 across various transformations, indicating a moderate to high degree of alignment between the estimated and true edited regions. For photometric and geometric reasoning, we first analyse the parameter estimates of each individual transformation across corresponding parameter spectra and then report traceability in terms of the average prediction error. Figure 7 presents the mean estimates with standard deviations over the parameter spectrum, where the diagonal line denotes perfect agreement with the ground truth. In photometric reasoning, the estimated hue parameters align closely with their ground-truth counterparts, whereas brightness, contrast and saturation exhibit larger deviations, particularly under stronger adjustments at the extremes. In geometric reasoning, the parameter estimations for rotation, translation, scaling and shearing are nearly perfect. Traceability is slightly degraded under composite transformations, where both photometric and geometric distortions are imposed following semantic synthesis. Table I summarises the average prediction errors for each class of transformation parameter under different

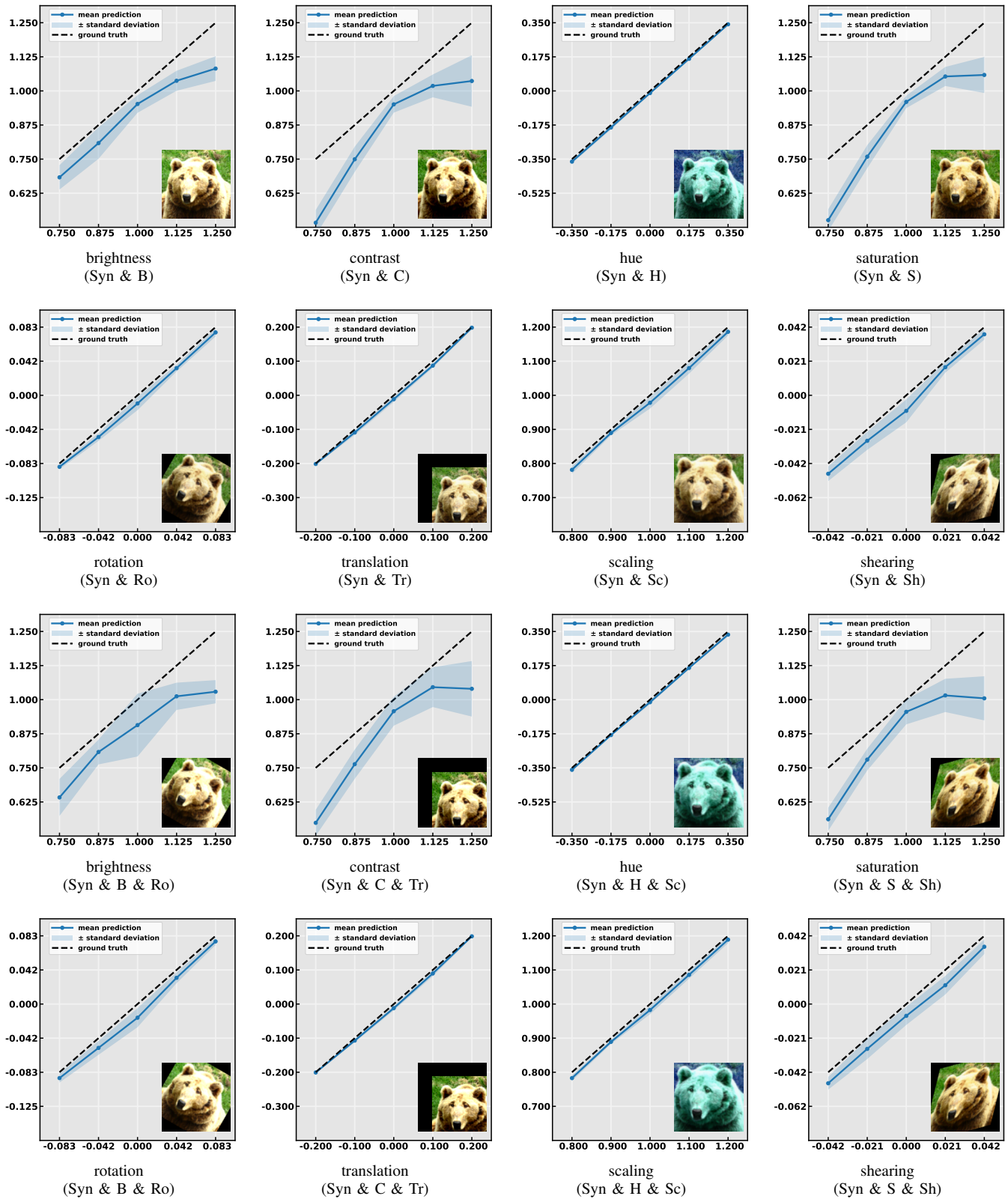


Fig. 7. Traceability evaluation of photometric and geometric reasoning based on deviations between estimated and true parameter values.

transformation chains. It is observed that geometric parameters are estimated with high accuracy, regardless of whether they are applied or not. Among the photometric parameters, hue exhibits the lowest and most stable errors, while brightness,

contrast and saturation show larger deviations, particularly when the parameter under evaluation is the one perturbed in the transformation chain. The results confirm the validity of tracing applied transformations through tell-tale watermarks.

TABLE I  
TRACEABILITY ACROSS TRANSFORMATIONS

		Average Prediction Error Per Transform							
		Brightness	Contrast	Hue	Saturation	Rotation	Translation	Scaling	Shearing
Applied Transform Chain	Syn & B	<b>0.0874</b>	0.0504	0.0120	0.0657	0.0108	0.0112	0.0246	0.0117
	Syn & C	0.0487	<b>0.1456</b>	0.0106	0.0458	0.0082	0.0107	0.0266	0.0087
	Syn & H	0.0479	0.0509	<b>0.0110</b>	0.0448	0.0096	0.0130	0.0248	0.0115
	Syn & S	0.0479	0.0420	0.0110	<b>0.1287</b>	0.0098	0.0101	0.0272	0.0096
	Syn & Ro	0.0424	0.0516	0.0278	0.0415	<b>0.0077</b>	0.0080	0.0128	0.0072
	Syn & Tr	0.0600	0.0645	0.0113	0.0665	0.0082	<b>0.0073</b>	0.0132	0.0093
	Syn & Sc	0.0430	0.0438	0.0126	0.0334	0.0097	0.0073	<b>0.0170</b>	0.0067
	Syn & Sh	0.0426	0.0445	0.0112	0.0378	0.0083	0.0087	0.0222	<b>0.0062</b>
	Syn & B & Ro	<b>0.1204</b>	0.0653	0.0378	0.0568	<b>0.0104</b>	0.0091	0.0180	0.0082
	Syn & C & Tr	0.0674	<b>0.1289</b>	0.0136	0.0577	0.0100	<b>0.0063</b>	0.0161	0.0077
	Syn & H & Sc	0.0406	0.0488	<b>0.0115</b>	0.0437	0.0083	0.0093	<b>0.0143</b>	0.0078
	Syn & S & Sh	0.0532	0.0513	0.0108	<b>0.1364</b>	0.0084	0.0104	0.0264	<b>0.0073</b>

## V. CONCLUSION

This study addressed the forensic challenge of reconstructing the latent transformation chain underlying synthetic media. Tell-tale watermarks are developed to remain synchronised with the transformation dynamics applied to their carrier media, permitting explanatory reasoning from the interpretable traces left behind. The reasoning process, however, is inherently constrained by the combinatorial explosion of possible transformation sequences, which limits scalability in unconstrained environments. The restriction to sequential order leaves open the broader problem of reconstructing the complete timeline of editing history. Future research may explore tell-tale watermark designs tailored or generalised to a wider range of transformations, thereby supporting traceability in the evolving landscape of synthetic media forensics.

## ACKNOWLEDGEMENTS

This work was supported in part by the Japan Society for the Promotion of Science (JSPS) under KAKENHI Grants (JP21H04907 and JP24H00732), and in part by the Japan Science and Technology Agency (JST) under CREST Grant (JPMJCR20D3) including AIP Challenge Program, AIP Acceleration Grant (JPMJCR24U3) and K Program Grant (JPMJKP24C2).

## REFERENCES

- B. Zhu, M. Swanson, and A. Tewfik, "When seeing isn't believing [multimedia authentication technologies]," *IEEE Signal Process. Mag.*, vol. 21, no. 2, pp. 40–49, 2004.
- S. J. Nightingale, K. A. Wade, and D. G. Watson, "Can people identify original and manipulated photos of real-world scenes?" *Cogn. Res. Princ. Implic.*, vol. 2, no. 1, pp. 1–21, 2017.
- R. Chesney and D. Citron, "Deepfakes and the new disinformation war," *Foreign Aff.*, vol. 98, no. 1, pp. 147–155, 2019.
- S. Greengard, "Will deepfakes do deep damage?" *Commun. ACM*, vol. 63, no. 1, pp. 17–19, 2019.
- I. Goodfellow *et al.*, "Generative adversarial networks," *Commun. ACM*, vol. 63, no. 11, pp. 139–144, 2020.
- Y. Mirsky and W. Lee, "The creation and detection of deepfakes: A survey," *ACM Comput. Surv.*, vol. 54, no. 1, pp. 1–41, 2021.
- J. Thies, M. Zollhöfer, M. Nießner, L. Valgaerts, M. Stamminger, and C. Theobalt, "Real-time expression transfer for facial reenactment," *ACM Trans. Graph.*, vol. 34, no. 6, pp. 1–14, 2015.
- A. Brock, T. Lim, J. M. Ritchie, and N. Weston, "Neural photo editing with introspective adversarial networks," in *Proc. Int. Conf. Learn. Represent. (ICLR)*, Toulon, France, 2017, pp. 1–15.
- H. Kim *et al.*, "Deep video portraits," *ACM Trans. Graph.*, vol. 37, no. 4, pp. 1–14, 2018.
- J. Thies, M. Zollhöfer, M. Stamminger, C. Theobalt, and M. Nießner, "Face2Face: Real-time face capture and reenactment of RGB videos," *Commun. ACM*, vol. 62, no. 1, pp. 96–104, 2018.
- O. Wiles, A. S. Koepke, and A. Zisserman, "X2Face: A network for controlling face generation using images, audio, and pose codes," in *Proc. Eur. Conf. Comput. Vis. (ECCV)*, Munich, Germany, 2018, pp. 690–706.
- L. Liu *et al.*, "Neural rendering and reenactment of human actor videos," *ACM Trans. Graph.*, vol. 38, no. 5, pp. 1–14, 2019, Art. no. 139.
- J. Thies, M. Elgharib, A. Tewari, C. Theobalt, and M. Nießner, "Neural voice puppetry: Audio-driven facial reenactment," in *Proc. Eur. Conf. Comput. Vis. (ECCV)*, Glasgow, UK, 2020, pp. 716–731.
- C. Saharia *et al.*, "Photorealistic text-to-image diffusion models with deep language understanding," in *Proc. Int. Conf. Neural Inf. Process. Syst. (NeurIPS)*, vol. 35, New Orleans, LA, USA, 2022, pp. 36 479–36 494.
- M. Del Vicario *et al.*, "The spreading of misinformation online," *Proc. Natl. Acad. Sci. USA*, vol. 113, no. 3, pp. 554–559, 2016.
- S. Lewandowsky, U. K. H. Ecker, and J. Cook, "Beyond misinformation: Understanding and coping with the "post-truth" era," *J. Appl. Res. Mem. Cogn.*, vol. 6, no. 4, pp. 353–369, 2017.
- D. M. J. Lazer *et al.*, "The science of fake news," *Science*, vol. 359, no. 6380, pp. 1094–1096, 2018.
- S. Vosoughi, D. Roy, and S. Aral, "The spread of true and false news online," *Science*, vol. 359, no. 6380, pp. 1146–1151, 2018.
- G. G. Richard and V. Roussev, "Next-generation digital forensics," *Commun. ACM*, vol. 49, no. 2, pp. 76–80, 2006.
- J. Fridrich, "Digital image forensics," *IEEE Signal Process. Mag.*, vol. 26, no. 2, pp. 26–37, 2009.
- H. Farid, "Image forgery detection," *IEEE Signal Process. Mag.*, vol. 26, no. 2, pp. 16–25, 2009.
- A. Rocha, W. Scheirer, T. Boult, and S. Goldenstein, "Vision of the unseen: Current trends and challenges in digital image and video forensics," *ACM Comput. Surv.*, vol. 43, no. 4, pp. 1–42, 2011.
- M. C. Stamm and K. R. Liu, "Forensic detection of image manipulation using statistical intrinsic fingerprints," *IEEE Trans. Inf. Forensics Secur.*, vol. 5, no. 3, pp. 492–506, 2010.
- P. Zhou, X. Han, V. I. Morariu, and L. S. Davis, "Learning rich features for image manipulation detection," in *Proc. IEEE/CVF Conf. Comput. Vis. Pattern Recognit. (CVPR)*, Salt Lake City, UT, USA, 2018, pp. 1053–1061.
- R. Zellers *et al.*, "Defending against neural fake news," in *Proc. Int. Conf. Neural Inf. Process. Syst. (NeurIPS)*, vol. 32, Vancouver, BC, Canada, 2019, pp. 9054–9065.
- F. Marra, D. Gragnaniello, L. Verdoliva, and G. Poggi, "Do GANs leave artificial fingerprints?" in *Proc. IEEE Conf. Multimedia Inf. Process. Retr. (MIPR)*, San Jose, CA, USA, 2019, pp. 506–511.
- P. Korus and N. Memon, "Computational sensor fingerprints," *IEEE Trans. Inf. Forensics Secur.*, vol. 17, pp. 2508–2523, 2022.
- E. Mitchell, Y. Lee, A. Khazatsky, C. D. Manning, and C. Finn, "DetectGPT: Zero-shot machine-generated text detection using probability curvature," in *Proc. Int. Conf. Mach. Learn. (ICML)*, vol. 202, Honolulu, HI, USA, 2023, pp. 24 950–24 962.

- [29] Y. Li, M.-C. Chang, and S. Lyu, "In icu oculi: Exposing AI created fake videos by detecting eye blinking," in *Proc. IEEE Int. Workshop Inf. Forensics Secur. (WIFS)*, Hong Kong, China, 2018, pp. 1–7.
- [30] X. Yang, Y. Li, and S. Lyu, "Exposing deep fakes using inconsistent head poses," in *Proc. IEEE Int. Conf. Acoust. Speech Signal Process. (ICASSP)*, Brighton, UK, 2019, pp. 8261–8265.
- [31] A. Rössler, D. Cozzolino, L. Verdoliva, C. Riess, J. Thies, and M. Niessner, "FaceForensics++: Learning to detect manipulated facial images," in *Proc. IEEE/CVF Int. Conf. Comput. Vis. (ICCV)*, Seoul, Korea, 2019, pp. 1–11.
- [32] U. A. Ciftci, I. Demir, and L. Yin, "FakeCatcher: Detection of synthetic portrait videos using biological signals," *IEEE Trans. Pattern Anal. Mach. Intell.*, pp. 1–1, 2020.
- [33] L. Li *et al.*, "Face X-ray for more general face forgery detection," in *Proc. IEEE/CVF Conf. Comput. Vis. Pattern Recognit. (CVPR)*, Seattle, WA, USA, 2020, pp. 5000–5009.
- [34] T. Zhou, W. Wang, Z. Liang, and J. Shen, "Face forensics in the wild," in *Proc. IEEE/CVF Conf. Comput. Vis. Pattern Recognit. (CVPR)*, Nashville, TN, USA, 2021, pp. 5774–5784.
- [35] A. Haliassos, K. Vougioukas, S. Petridis, and M. Pantic, "Lips don't lie: A generalisable and robust approach to face forgery detection," in *Proc. IEEE/CVF Conf. Comput. Vis. Pattern Recognit. (CVPR)*, Nashville, TN, USA, 2021, pp. 5037–5047.
- [36] K. Shiohara and T. Yamasaki, "Detecting deepfakes with self-blended images," in *Proc. IEEE/CVF Conf. Comput. Vis. Pattern Recognit. (CVPR)*, New Orleans, LA, USA, 2022, pp. 18 699–18 708.
- [37] F. Guilaro, D. Cozzolino, A. Sud, N. Dufour, and L. Verdoliva, "TruFor: Leveraging all-round clues for trustworthy image forgery detection and localization," in *Proc. IEEE/CVF Conf. Comput. Vis. Pattern Recognit. (CVPR)*, Vancouver, BC, Canada, 2023, pp. 20 606–20 615.
- [38] G. Friedman, "The trustworthy digital camera: Restoring credibility to the photographic image," *IEEE Trans. Consum. Electron.*, vol. 39, no. 4, pp. 905–910, 1993.
- [39] M. D. Swanson, M. Kobayashi, and A. H. Tewfik, "Multimedia data-embedding and watermarking technologies," *Proc. IEEE*, vol. 86, no. 6, pp. 1064–1087, 1998.
- [40] F. Petitcolas, R. Anderson, and M. Kuhn, "Information hiding—A survey," *Proc. IEEE*, vol. 87, no. 7, pp. 1062–1078, 1999.
- [41] F. Hartung and M. Kutter, "Multimedia watermarking techniques," *Proc. IEEE*, vol. 87, no. 7, pp. 1079–1107, 1999.
- [42] G. Voyatzis and I. Pitas, "The use of watermarks in the protection of digital multimedia products," *Proc. IEEE*, vol. 87, no. 7, pp. 1197–1207, 1999.
- [43] I. J. Cox, M. L. Miller, and A. L. McKellips, "Watermarking as communications with side information," *Proc. IEEE*, vol. 87, no. 7, pp. 1127–1141, 1999.
- [44] C.-C. Chang, H. H. Nguyen, J. Yamagishi, and I. Echizen, "Cyber vaccine for deepfake immunity," *IEEE Access*, vol. 11, pp. 105 027–105 039, 2023.
- [45] I. J. Cox, J. Kilian, F. T. Leighton, and T. Shamon, "Secure spread spectrum watermarking for multimedia," *IEEE Trans. Image Process.*, vol. 6, no. 12, pp. 1673–1687, 1997.
- [46] M. Barni, F. Bartolini, V. Cappellini, and A. Piva, "A DCT-domain system for robust image watermarking," *Signal Process.*, vol. 66, no. 3, pp. 357–372, 1998.
- [47] R. Liu and T. Tan, "An SVD-based watermarking scheme for protecting rightful ownership," *IEEE Trans. Multimed.*, vol. 4, no. 1, pp. 121–128, 2002.
- [48] X. Luo, R. Zhan, H. Chang, F. Yang, and P. Milanfar, "Distortion agnostic deep watermarking," in *Proc. IEEE/CVF Conf. Comput. Vis. Pattern Recognit. (CVPR)*, Seattle, WA, USA, 2020, pp. 13 545–13 554.
- [49] J. Kirchenbauer, J. Geiping, Y. Wen, J. Katz, I. Miers, and T. Goldstein, "A watermark for large language models," in *Proc. Int. Conf. Mach. Learn. (ICML)*, vol. 202, Honolulu, HI, USA, 2023, pp. 17 061–17 084.
- [50] P. Fernandez, G. Couairon, H. Jégou, M. Douze, and T. Furon, "The stable signature: Rooting watermarks in latent diffusion models," in *Proc. IEEE/CVF Int. Conf. Comput. Vis. (ICCV)*, Paris, France, 2023, pp. 22 409–22 420.
- [51] R. S. Roman, P. Fernandez, H. Elshar, A. Défossez, T. Furon, and T. Tran, "Proactive detection of voice cloning with localized watermarking," in *Proc. Int. Conf. Mach. Learn. (ICML)*, Vienna, Austria, 2024, pp. 43 180–43 196.
- [52] S. Dathathri *et al.*, "Scalable watermarking for identifying large language model outputs," *Nature*, vol. 634, no. 8035, pp. 818–823, 2024.
- [53] M. Yeung and F. Mintzer, "An invisible watermarking technique for image verification," in *Proc. Int. Conf. Image Process. (ICIP)*, vol. 2, Santa Barbara, CA, USA, 1997, pp. 680–683.
- [54] J. Fridrich, "Image watermarking for tamper detection," in *Proc. IEEE Int. Conf. Image Process. (ICIP)*, vol. 2, Chicago, IL, USA, 1998, pp. 404–408.
- [55] M. Wu and B. Liu, "Watermarking for image authentication," in *Proc. Int. Conf. Image Process. (ICIP)*, vol. 2, Chicago, IL, USA, 1998, pp. 437–441.
- [56] P. W. Wong and N. Memon, "Secret and public key image watermarking schemes for image authentication and ownership verification," *IEEE Trans. Image Process.*, vol. 10, no. 10, pp. 1593–1601, 2001.
- [57] Y. Zhao, B. Liu, M. Ding, B. Liu, T. Zhu, and X. Yu, "Proactive deepfake defence via identity watermarking," in *Proc. IEEE/CVF Winter Conf. Appl. Comput. Vis. (WACV)*, Waikoloa, HI, USA, 2023, pp. 4591–4600.
- [58] P. Neekhar, S. Hussain, X. Zhang, K. Huang, J. McAuley, and F. Koushanfar, "FaceSigns: Semi-fragile watermarks for media authentication," *ACM Trans. Multimedia Comput. Commun. Appl.*, vol. 20, no. 11, pp. 1–21, 2024.
- [59] Y. Zhao, B. Liu, T. Zhu, M. Ding, X. Yu, and W. Zhou, "Proactive image manipulation detection via deep semi-fragile watermark," *Neurocomputing*, vol. 585, pp. 1–14, 2024.
- [60] D. Moreira *et al.*, "Image provenance analysis at scale," *IEEE Trans. Image Process.*, vol. 27, no. 12, pp. 6109–6123, 2018.
- [61] A. Bharati *et al.*, "Beyond pixels: Image provenance analysis leveraging metadata," in *Proc. IEEE Winter Conf. Appl. Comput. Vis. (WACV)*, Waikoloa, HI, USA, 2019, pp. 1692–1702.
- [62] X. Zhang, Z. H. Sun, S. Karaman, and S.-F. Chang, "Discovering image manipulation history by pairwise relation and forensics tools," *IEEE J. Sel. Top. Signal Process.*, vol. 14, no. 5, pp. 1012–1023, 2020.
- [63] C. Pasquini, I. Amerini, and G. Boato, "Media forensics on social media platforms: A survey," *EURASIP J. Inf. Secur.*, pp. 1–19, 2021.
- [64] X. Jin *et al.*, "MFC-Prov: Media forensics challenge image provenance evaluation and data analysis on large-scale datasets," *Neurocomputing*, vol. 470, pp. 76–88, 2022.
- [65] F. Breiting, H. Studiawan, and C. Hargreaves, "SoK: Timeline based event reconstruction for digital forensics: Terminology, methodology, and current challenges," *Forensic Sci. Int. Digit. Investig.*, vol. 53, pp. 1–15, 2025.
- [66] I. Niiniluoto, "Abduction, tomography, and other inverse problems," *Stud. Hist. Philos. Sci. A*, vol. 42, no. 1, pp. 135–139, 2011.
- [67] G. H. Harman, "The inference to the best explanation," *Philos. Rev.*, vol. 74, no. 1, pp. 88–95, 1965.
- [68] D. Kundur and D. Hatzinakos, "Digital watermarking for telltale tamper proofing and authentication," *Proc. IEEE*, vol. 87, no. 7, pp. 1167–1180, 1999.
- [69] T.-Y. Lin *et al.*, "Microsoft COCO: Common objects in context," in *Proc. Eur. Conf. Comput. Vis. (ECCV)*, Zurich, Switzerland, 2014, pp. 740–755.
- [70] O. Ronneberger, P. Fischer, and T. Brox, "U-Net: Convolutional networks for biomedical image segmentation," in *Proc. Int. Conf. Med. Image Comput. Comput.-Assist. Interv. (MICCAI)*, Cham, 2015, pp. 234–241.
- [71] K. He, X. Zhang, S. Ren, and J. Sun, "Deep residual learning for image recognition," in *Proc. IEEE Conf. Comput. Vis. Pattern Recognit. (CVPR)*, Las Vegas, NV, USA, 2016, pp. 770–778.
- [72] S. Woo, J. Park, J.-Y. Lee, and I. S. Kweon, "CBAM: Convolutional block attention module," in *Proc. Eur. Conf. Comput. Vis. (ECCV)*, Munich, Germany, 2018, pp. 3–19.
- [73] R. Rombach, A. Blattmann, D. Lorenz, P. Esser, and B. Ommer, "High-resolution image synthesis with latent diffusion models," in *Proc. IEEE/CVF Conf. Comput. Vis. Pattern Recognit. (CVPR)*, New Orleans, LA, USA, 2022, pp. 10 674–10 685.